Journal of Biomechanics 85 (2019) 173–181

Contents lists available at ScienceDirect

Journal of Biomechanics

journal homepage: www.elsevier.com/locate/jbiomech
www.JBiomech.com

A principal component analysis-based framework for statistical modeling of bone displacement during wrist maneuvers

Brent H. Foster [a], Calvin B. Shaw [b], Robert D. Boutin [b], Anand A. Joshi [c], Christopher O. Bayne [d], Robert M. Szabo [d], Abhijit J. Chaudhari [b,*]

[a] Department of Biomedical Engineering, University of California Davis, Davis, CA 95616, USA
[b] Department of Radiology, University of California Davis School of Medicine, Sacramento, CA 95817, USA
[c] Signal and Image Processing Institute, University of Southern California, Los Angeles, CA 90089, USA
[d] Department of Orthopedic Surgery, University of California Davis School of Medicine, Sacramento, CA 95817, USA

ARTICLE INFO

Article history:
Accepted 16 January 2019

Keywords:
Wrist bone displacement
Statistical modeling
Principal component analysis
Sex differences

ABSTRACT

We present a method for the statistical modeling of the displacements of wrist bones during the performance of coordinated maneuvers, such as radial-ulnar deviation (RUD). In our approach, we decompose bone displacement via a set of basis functions, identified via principal component analysis (PCA). We utilized MRI wrist scans acquired at multiple static positions for deriving these basis functions. We then utilized these basis functions to compare the displacements undergone by the bones of the left versus right wrist in the same individual, and between bones of the wrists of men and women, during the performance of the coordinated RUD maneuver. Our results show that the complex displacements of the wrist bones during RUD can be modeled with high reliability with just 5 basis functions, that captured over 91% of variation across individuals. The basis functions were able to predict intermediate wrist bone poses with an overall high accuracy (mean error of 0.26 mm). Our proposed approach found statistically significant differences between bone displacement trajectories in women versus men, however, did not find significant differences in those of the left versus right wrist in the same individual. Our proposed method has the potential to enable detailed analysis of wrist kinematics for each sex, and provide a robust framework for characterizing the normal and pathologic displacement of the wrist bones, such as in the context of wrist instability.

1. Introduction

Normal wrist function is facilitated by a complex interplay between the eight carpal bones, the radius and ulna bones, and their associated ligaments, the latter constraining bone displacement during motion and providing stability. There remain gaps in our knowledge on how the bones of the wrist move, highlighted by the lack of a consensus on a unified theory of wrist bone displacement during motion (Moojen et al., 2003; Sandow et al., 2014). Current techniques typically assess rotational and translational measures associated with local displacement for each individual wrist bone independently during the performance of a specific wrist maneuver (Foumani et al., 2009; Garcia-Elias et al., 2014; Moojen et al., 2003; Rainbow et al., 2016; Sonenblum et al., 2004; Waters et al., 2016). This approach may be inadequate, as it does not account for how the displacement of a particular bone may influence other bones. On the other hand, current studies that represent carpal motion via "average" kinematics may not take into consideration the variance in the displacement of individual bones during a coordinated wrist maneuver (Chen et al., 2013).

A statistical model that capitalizes on the correlative relationship between wrist bone displacement could potentially improve our understanding of wrist kinematics and have the ability to compare bone motion of the entire wrist between different groups. In particular, there are two notable comparisons the model would enable. First, it would be helpful in understanding if and how carpal bone displacement is influenced by sex, as there appears to be a lack of consensus regarding whether the carpal bone displacement pattern is sex-dependent (such as with the row/column wrist theory (Craigen and Stanley, 1995; Galley et al., 2007; Sandow et al., 2014)) or independent (Rainbow et al., 2008). Second, it would test if carpal bone trajectories for the left and right wrist of the same individual differ. Knowledge of sex-based and/or wrist laterality-based differences may allow for more personalized surgical

* Corresponding author at: Department of Radiology, University of California Davis, 4860 Y Street, Suite 3100, Sacramento, CA 95817, USA.
E-mail address: ajchaudhari@ucdavis.edu (A.J. Chaudhari).

https://doi.org/10.1016/j.jbiomech.2019.01.030
0021-9290/

reconstruction, confirm the validity of using the opposite wrist for assessing altered kinematics whether from injury or after repair, and may be useful for future biomechanical studies of wrist motion.

We propose a method for creating such a model, using principal component analysis (PCA), to describe the trajectory of the bones of the wrist during the performance of a coordinated maneuver, the radial-ulnar deviation (RUD). The method uses PCA to calculate basis functions (eigenvectors), i.e. the principal directions of displacement, and encodes model complexity and displacement-based spatial correlations between the bones in terms of model coefficients. We employed data from MRI scans of the right and left wrists of healthy individuals to construct the basis functions. We then demonstrate the ability of the proposed method for testing the following hypotheses during the performance of the coordinated maneuver (RUD): (1) there are no differences in the model coefficients between wrists of men and women; and (2) there are no differences in the model coefficients between the right and left wrists of the same individual. Testing these hypotheses will provide useful information to understand the biomechanical behavior of the wrist joints during the performance of coordinated maneuvers. Finally, we demonstrate that the method is able to create an 'individual model' which can retain information associated with each individual's wrist bone displacement during performance of a maneuver, while also modeling group displacement.

2. Methods

2.1. Wrist MRI protocol

Institutional review board (IRB) approval was obtained for the study and written informed consent was obtained from all study participants. Data were acquired on a 3.0 T system (Skyra, Siemens Healthcare, Erlangen, Germany), using a 32-channel brain radiofrequency coil. The study population consisted of 9 men (age: 33.1 ± 5.8 yrs) and 9 women (age: 27.7 ± 9.9 yrs), with no history of injury, pain or pathology in either wrists. Both wrists were imaged sequentially in three static positions, namely, (i) extreme radial deviation (RD), (ii) neutral, and (iii) extreme ulnar deviation (UD) positions. A subset of the volunteers (N = 3 men and N = 5 women, 16 wrists) had two additional positions: (iv) between RD and neutral position, and (v) between neutral and UD position, for validating predicted bone displacement interpolated from modeling. The volunteers were provided specific instructions and a demonstration of positions outside the scanner. During image acquisition, the only constraint on the hand was a standardized flat plastic surface underneath in order to obtain more natural wrist positions. The MRI acquisition used a 3D T_1-weighted gradient recalled echo pulse sequence (called volumetric interpolated breath-hold examination with water excitation by the scanner vendor (Foster et al., 2017)) which provided good contrast of the bones of the wrist, see Fig. 1. The scan in the wrist's neutral position was acquired at a higher spatial resolution (voxel size of $0.47 \times 0.47 \times 0.5$ mm, acquisition time ~6 min per wrist) to enable improved bone surface segmentation (Foster et al., 2017). All the other positions were acquired at a lower spatial resolution to decrease the acquisition time and had a voxel size of $1.0 \times 1.0 \times 1.0$ mm (~2 min per wrist).

Four (N = 3 men and N = 1 woman) participants returned for a repeat scan at an average of one month after their first scan for assessing scan-rescan reliability. They were provided with the same instructions as their first scan and were scanned for three positions of their right wrist.

2.2. Data creation for PCA-based basis function determination

In Fig. 2 we summarize the creation of training data to determine the basis functions from PCA. Specifically, we semi-automatically segmented the 8 carpal bones, the radius, and the ulna in each T_1-weighted scan position using the WRist Image Segmentation Toolkit (WRIST) (Foster et al., 2017) within 3D Slicer which provided 30 segmented surfaces per wrist per individual

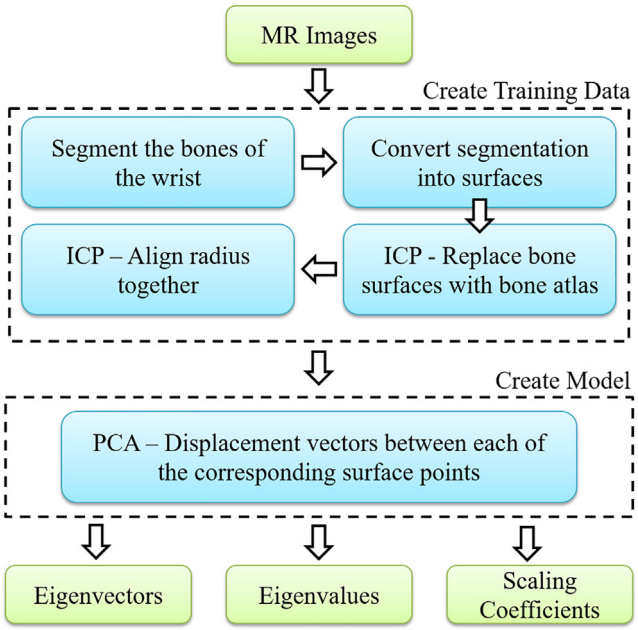

Fig. 2. Flowchart for constructing the PCA-based basis functions and creating the motion model.

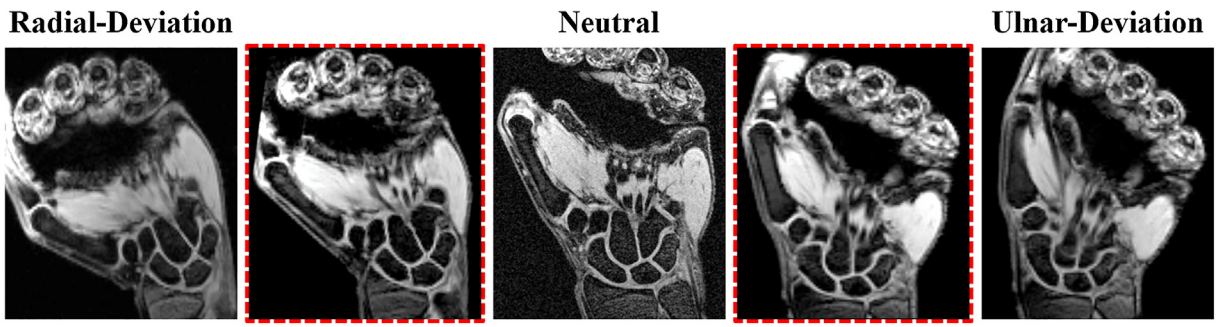

Fig. 1. Representative T_1-weighted images of one volunteer in the various static positions. All volunteers (N = 18, 36 wrists) were imaged in the extreme RD, neutral, and extreme UD positions while a subset (N = 8, 16 wrists) was also imaged in halfway positions, outlined in red above. (For interpretation of the references to color in this figure legend, the reader is referred to the web version of this article.)

(10 bones times 3 positions), see Fig. 3. Standard surface smoothing was performed using morphological operators to overcome topological inconsistencies (Chaudhari et al., 2014). For simplicity, the left wrist segmentations were mirrored (to match the overall orientation of the right wrist) (Schneider et al., 2015).

Next, we needed to remove the inter-subject bone shape differences from the training data since the bone shape differences would confound the displacement vectors for training the PCA model. In other words, all volunteers needed to have the same bone shapes while maintaining the original bone orientation and position. We randomly chose one participant's bone from their right wrist MRI to be the template bone shapes, and all the volunteer bones were replaced with the template bone shapes using a rigid iterative closest point (ICP) surface registration approach. Our assumption here was that given the non-spherical shape of the bones, the ICP-registered template bone matched the center of mass and the orientation of the principal axis of each person's bone relatively accurately. This process allowed us to remove the inter-subject bone shape differences while accurately maintaining the correct bone location and orientation for each position of each individual.

Next, the radius bone of each set of segmented bones was aligned with the radius bone of the template in the neutral position, also using a rigid ICP-based approach. The affine transform matrix generated during registration of the radius was then applied to all the bones to bring them into the coordinate system of the template, with the radius bone as an anchor. We chose the radius bone as an anchor because global bone displacement during maneuvers is commonly considered with respect to the radius (Coburn et al., 2007; Wu et al., 2005). Alternatively, any bone of the wrist can be chosen as an anchor in our method, as we demonstrate in our analysis of the scaphoid and lunate displacement, with the capitate bone as an anchor (see supplementary materials). Lastly, the radial-to-ulnar deviation angle was calculated for normalizing variations in positioning, see supplementary materials for details of this measurement.

2.3. Derivation of PCA-based basis functions (eigenfunctions)

Shapes consisting of n points in k dimensions were concatenated into a kn-vector (Stegmann and Gomez, 2002). Specifically for our bone surfaces, $k = 3$, then

$$\boldsymbol{x} = [x_1, \ldots, x_n, y_1, \ldots, y_n, z_1, \ldots, z_n]^T. \quad (1)$$

Similarly, multiple bone shapes were concatenated within this vector to have a single vector $\boldsymbol{x}$ which represents the 3D position of the ten bones of the wrist, i.e. N positions of the wrist bones were represented by $\boldsymbol{x}_1, \boldsymbol{x}_2, \ldots, \boldsymbol{x}_N$. In this study, N was three positions per volunteer, but additional positions could be easily incorporated into the model. For our analysis, the bone shapes which comprise this concatenated $\boldsymbol{x}$ remained the same between all time points (i.e. wrist positions) while the translation and rotation of the bones varied, see Fig. 3.

The mean position of the surface vertices (all wrist bones) was computed by a simple averaging over the N positions, i.e.,

$$\bar{\boldsymbol{x}} = \frac{1}{N}\sum_{i=1}^{N}\boldsymbol{x}_i, \quad (2)$$

where $\bar{\boldsymbol{x}}$ is the mean position of the bone surfaces, similar to finding the mean shape in statistical shape analysis (Heimann and Meinzer, 2009).

The covariance matrix based on the N positions is then given by

$$C = \frac{1}{N-1}\sum_{i=1}^{N}(\boldsymbol{x}_i - \bar{\boldsymbol{x}})(\boldsymbol{x}_i - \bar{\boldsymbol{x}})^T, \quad (3)$$

where $(\boldsymbol{x}_i - \bar{\boldsymbol{x}})$ represents the points of the wrist bones at position i minus the corresponding points on the mean wrist position. The covariance matrix represents displacement vectors from the mean wrist position ($\bar{\boldsymbol{x}}$) to each surface point at the position i. Note that due to concatenation, the covariance matrix also encodes covariance between the x, y, and z coordinates of the points.

The PCA algorithm (Wold et al., 1987) was then applied to produce an eigen-decomposition on C to find the modes of variation (i.e. basis functions or eigenvectors $\boldsymbol{\phi}_i$) and their respective variances (i.e. eigenvalues λ_i) (Xia et al., 2013). There are two likely benefits of this approach; first, there will be the opportunity for dimensionality reduction (given that bone displacement is expected to be relatively smooth (Stegmann and Gomez, 2002; Xia et al., 2013)); and second, an approximate new valid bone positions $\boldsymbol{x}$, not in the data set within the kinematic constraints of the training dataset and model (Xia et al., 2013), can be constructed via a linear combination of the basis functions, i.e.

$$\boldsymbol{x} = \bar{\boldsymbol{x}} + \sum_{i=1}^{N-1}\alpha_i\sqrt{\lambda_i}\boldsymbol{\phi}_i, \quad (4)$$

where α_i is the scaling (or weighing) term for the corresponding eigenvector. The α terms will be referred to as the model coefficients throughout this paper. The reliability for PCA-based basis functions derivation with varying number of scans was estimated via rigorous bootstrap analysis (Fisher et al., 2016) (please see the supplementary materials).

2.4. Modeling wrist bone displacement at positions not in the training data

In the $N = 8$ volunteers (16 wrists) scanned at two intermediate positions (between the RU and neutral, and UD and neutral), we

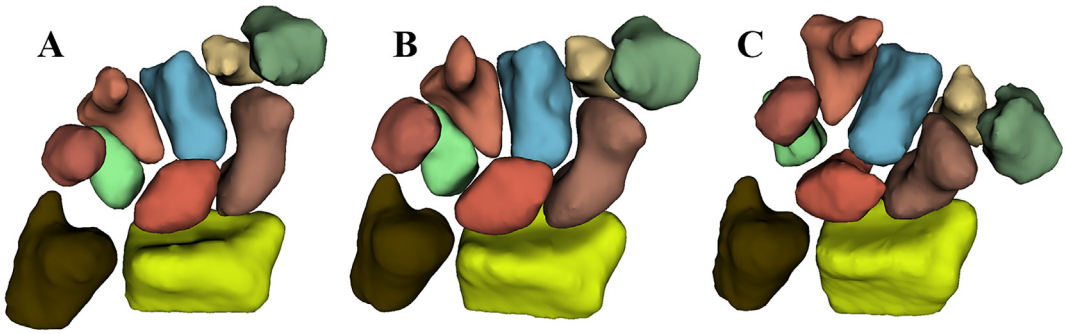

Fig. 3. Representative surfaces of the wrist bones used for creating the statistical model in the (A) UD, (B) neutral, and (C) RD positions for a study participant. PCA was employed to construct basis functions based on bone displacement between the positions.

assessed the capability of our basis functions to estimate these intermediate positions not part of basis function determination, utilizing Eq. (4). After model fitting, we quantified the accuracy by calculating the mean and maximum Euclidean distance between the corresponding points of the estimated model and those derived directly from the intermediate position being tested.

Further, for each eigenvector, a second-order polynomial model was fitted to each set of the model coefficients to enable them to estimate a trajectory of bone displacement through eigenspace. Renderings were then used to visually verify that realistic motion could be modeled by interpolating through the model coefficients in eigenspace.

2.5. Method implementation

We implemented the proposed method as an extension (application) in the open-source NIH-supported 3D Slicer tool that will be available on Github at https://github.com/AJChaudhari/PCA-Kinematics upon acceptance of this manuscript (more information in supplementary materials).

2.6. Experiments

2.6.1. Comparison of the model coefficients for the right and left wrists

Using only the MRI scans of the right wrists in their 3 positions, we determined the basis functions based on PCA. Once the basis functions were chosen, bones of both right and left wrist in the different orientations were projected onto the basis functions to obtain the corresponding model coefficients as well as the RUD angle of each position. We then computed the Pearson correlation coefficient between the model coefficients of the right versus left wrist. Lastly, a one-sample Hotelling's t-square test with pairing was used to compare the first five model coefficients of the right versus left wrist of the same individual.

2.6.2. Scan - rescan reliability

From the repeat scans of the N = 4 participants, bone surfaces were extracted. The basis functions computed above and model coefficients for the first and second scans were compared. This procedure allowed us to determine the robustness of the method to changes in the overall volunteer position and to other changes such as volunteer experience in the scanner.

2.6.3. Comparison of model coefficients between men versus women

The model coefficients were calculated separately for men and women (N = 9 of each sex), again using the basis functions derived earlier. Since the radial and ulnar deviation angles varied between volunteers during data acquisition, the model coefficients for each volunteer along with the measured angle of RUD were used to fit a second-order quadratic model between the positions using Eq. (4). Then, at eight RUD angles (50°, 60°, 70°, 80°, 90°, 100°, 110°, and 120° with respect to the line intersecting the radial styloid process and the distal radius sigmoid notch) across the range of motion, the model coefficients for each volunteer were computed. Our rationale, verified from studies in Section 2.4, was that an accurate estimation of the motion can be determined using the model coefficients derived from a predictable path through basis function space, found by interpolating between the model coefficients from the available positions. This procedure allowed for a comparable RUD angle between the volunteers, and a more meaningful comparison. The median model coefficient for each wrist angle was used for creating a visualization of the wrist positions for men and women. Lastly, a MANOVA was used to compare model coefficients between men and women.

3. Results

3.1. PCA-based basis function determination

Fig. 4 shows a rendering of the first and second principal directions derived from our data. Please see supplementary Movie 1 for an animation of the motion estimated via interpolation in eigenspace. All other model coefficients were set to zero except for the one indicated. This figure demonstrates that the first basis function indicated the RUD direction, as expected. The second basis function appeared to be a combination of wrist scaling, where a smaller coefficient represented a larger wrist (with larger spacing between the bones) and vice versa, and of flexion-extension, where a more positive scaling factor referred to extension while a more negative coefficient referred to flexion. The third basis function presented movement in the dorsal-radial to volar-ulnar direction, with mild RUD, and the fourth basis function had minimal residual motion in oblique RUD direction. Lastly, the fifth basis function showed an increased distal radial-ulnar joint distance with a notable increase in the ulnar rotation and translation about the radius bone.

3.2. Variance explained by basis functions

The variance explained for each eigenvector was quantified and plotted in Fig. 5. Overall, we found that the first five eigenvectors accounted for 93% of the variation with continued decreasing contributions past the first five, when using the N = 18 right wrists. Bootstrapping analysis (supplementary materials) with as low as 5 right wrist scans showed that five eigenvectors still captured variation in the range from 91.1% to 94.7%. In the scan-rescan setting, we found an excellent agreement between the model coefficients with a correlation coefficient of 0.92 ± 0.07 for the first five model coefficients (please see supplementary materials).

3.3. Model coefficients and pose estimation

In Fig. 6, the unique trajectory of the bones of a participant's wrist is shown (based on Eq. (4)), sampled at five RUD angles. Subtle flexion-extension was visualized for some, but not all, participants, highlighting the benefits of our approach.

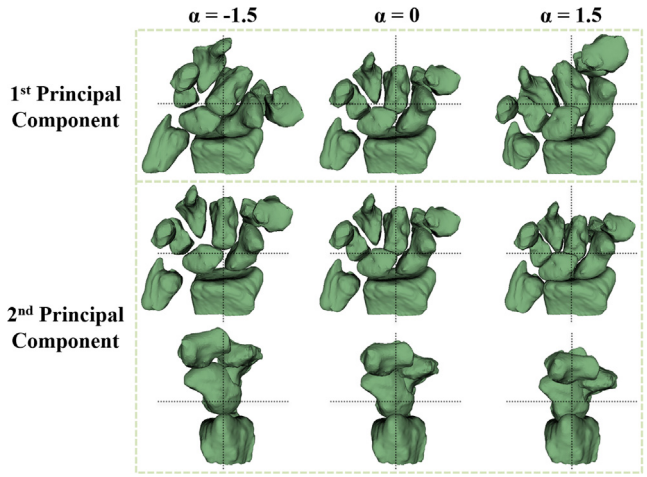

Fig. 4. Rendering of the first two principal components for the RUD motion. The α term refers to the model coefficient, and the first and second principal components were varied separately, i.e. all other model coefficients were set to zero. The first component was in the expected RUD direction while the second component was a combination of flexion-extension and bone spacing scaling. The dotted lines are intended to aid in visually comparing the bone positions between each row.

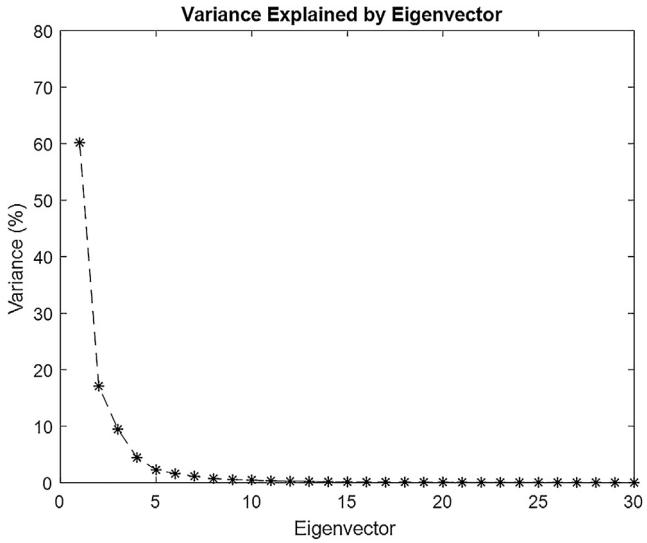

Fig. 5. Percent variance explained by each eigenvector (N = 18 right wrists). The total number of eigenvectors was the number of right wrist positions minus 1, i.e., $(18 \times 3) - 1$.

3.4. Model fit to the wrist positions not in the data used to derive the basis functions

The model was used to predict the 16 intermediate wrist positions, and the mean Euclidean distance between corresponding surface points was found to be 0.26 ± 0.09 mm, while the maximum distance between the corresponding landmarks was found to be 1.01 ± 0.34 mm. A representative example is visualized in Fig. 7. This high prediction accuracy suggests that the intermediate positions of the wrist bones can be estimated reliably by our proposed model.

3.5. Comparison of model coefficients for the right and left wrist

Fig. 8 show a plot of the first model coefficient for the right versus left wrists for 4 representative study participants. We found that this model coefficient had a linear relationship with the RUD angle, as expected. For the first 5 model coefficients, we found a Pearson correlation coefficient of 0.97 ± 0.03 between the trajectories of the right and left wrist bones, after adjusting for RUD angle, indicating a high level of similarity. The one-sample Hotelling's t-square test showed no statistically significant difference for the right versus left wrist model coefficients ($p = 0.15$).

3.6. Comparison of model coefficients between men and women

Eq. (4) and the model coefficients for the known wrist positions were used to generate wrist bone orientations at 8 RUD angles. Fig. 9 shows box plots for the first five model coefficients in men versus women. The first model coefficient had a linear relationship with RUD angle for both men and women, as also demonstrated earlier in Fig. 8. The second model coefficients had a quadratic relationship with RUD angle, and appeared to explain a subtle flexion-extension of the wrist during the RUD maneuver. The higher values for women for the second model coefficient are likely due to their smaller wrist sizes compared with men, and their larger range of flexion-extension. The third, fourth and fifth model coefficients appear to be mainly fitting a particular wrist and are fairly constant throughout the positions. The median value for each angle is rendered in 3D in Fig. 10 to visualize sex-specific differences.

When comparing the first 5 model coefficients individually, we applied corrections to the p-values to control for false discovery rate with multiple comparisons using the Benjamini and Hochberg procedure (Benjamini and Hochberg, 1995), which gave a corrected critical p-value of 0.02. The second, fourth, and fifth model coefficients had a p-value < 0.02, while the first and third did not. The first model coefficient, which was sensitive to displacement in the RUD direction, was not statistically different based on sex. The second principal direction was sensitive to both overall wrist bone size and displacement in the flexion-extension direction, and showed a difference by sex.

4. Discussion

We propose a method employing PCA to derive the basis functions of wrist bone displacement, which may help simplify kinematic analysis. In particular, the method is able to statistically compare the bone displacements of the entire joint between different groups of wrists, a large advantage over current methods which typically compare a single bone at a time. In comparison to existing methods, the proposed approach is data-driven without prior assumptions of the bone displacements (Wolfe et al., 2000), takes advantage of correlations in the bone displacements (Kawanishi et al., 2017; Rainbow et al., 2013), uses a small number of coefficients for simplified comparison and description (Foumani et al., 2009), describes the displacement of the entire wrist (Garcia-Elias

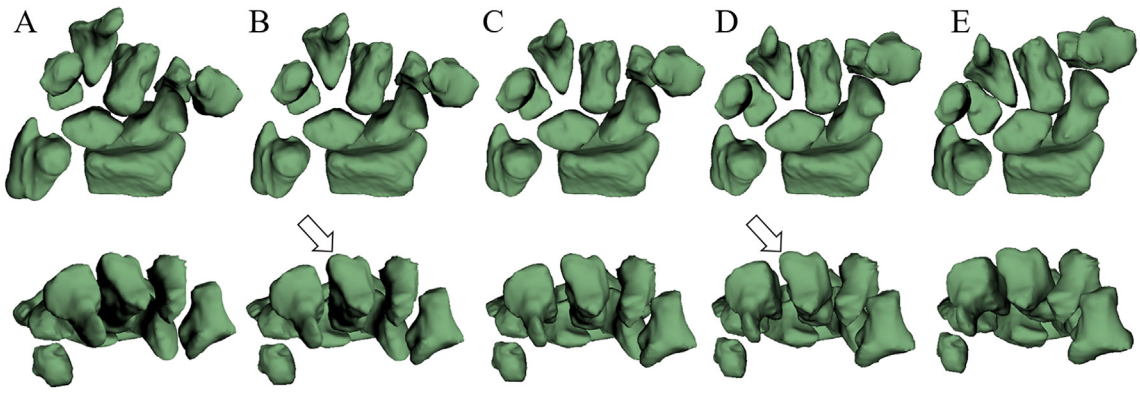

Fig. 6. Rendering of the individual kinematic model of one of the volunteers. Subtle flexion-extension was observed during the RUD maneuver in some volunteers, such as the one shown above. The positions rendered are (A) extreme RD, (B) halfway between extreme RD and neutral, (C) neutral, (D) halfway between neutral and extreme UD, and (E) extreme UD. Top row is a volar view of the wrist, while the bottom row is a top down view. The arrows indicate subtle flexion-extension.

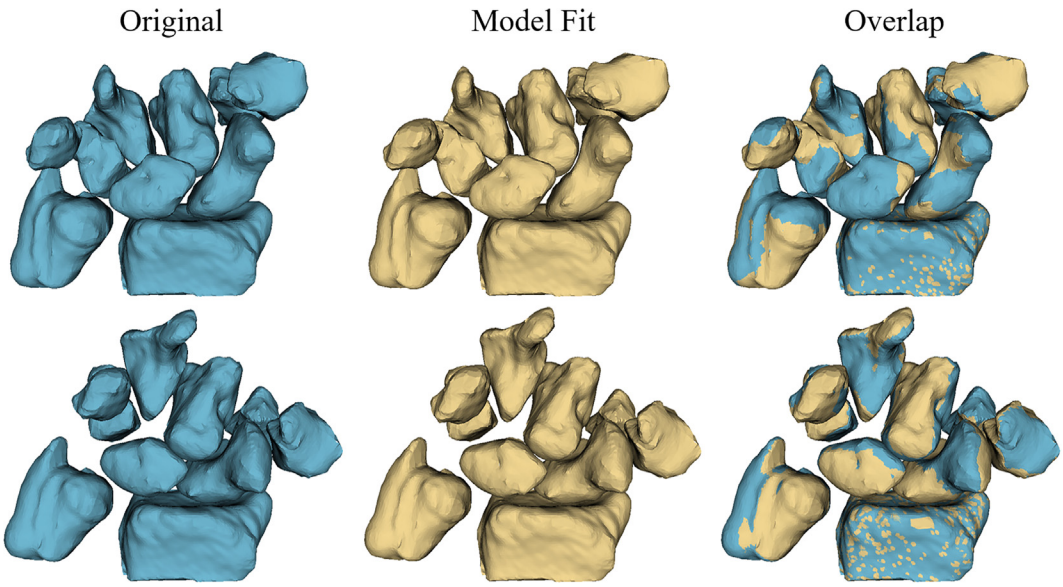

Fig. 7. Example prediction of the bone displacement model to the intermediate positions from one volunteer mid-way between neutral and UD (top row) and mid-way between neutral and RD (bottom row) positions. "Original" (far left column) refers to surfaces of the intermediate positions, after bone atlas alignment. "Model Prediction" (middle column) are the bone positions predicted by the model. "Overlap" (right column) refers to the overlay of the "Original" and "Model Prediction" bone surfaces. The mean Euclidean distance in this case was 0.24 ± 0.20 mm.

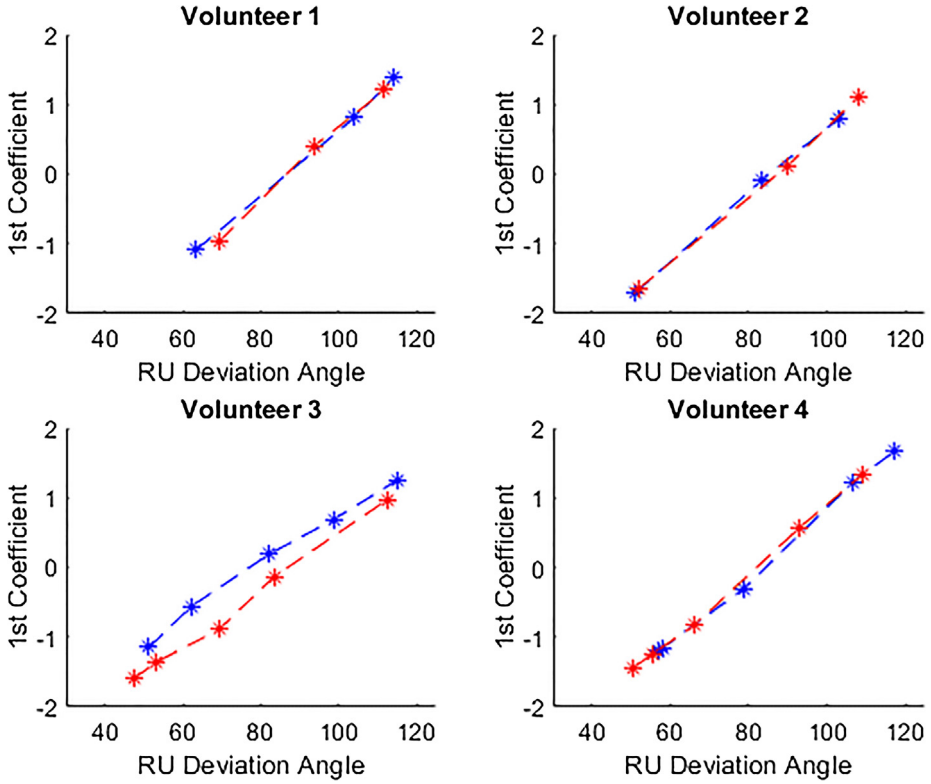

Fig. 8. The model coefficients between the right wrist (plotted in red) and the left wrist (plotted in blue) versus the RUD angle for 4 representative volunteers. Lower RUD angles refer to more radial deviation while higher RUD angles refer to more ulnar deviation. (For interpretation of the references to color in this figure legend, the reader is referred to the web version of this article.)

et al., 2014; Neu et al., 2001; Werner et al., 2011), and has an extendable framework (Moojen et al., 2003).

The data-driven approach led to a robust model without the need to specify any prior information on the basis functions, and we demonstrated that complex bone displacement during wrist RUD can be comprehensively summarized, capturing over 91% variation, using only 5 basis functions/coefficients. These basis functions provide information on correlated adjacent bone motion in order of relative importance and may lead to insights for creating new unified theories of wrist motion. The basis functions will likely also be useful in classifying wrist phenotypes by analyzing which basis functions have larger weighing factors, i.e. the PCA

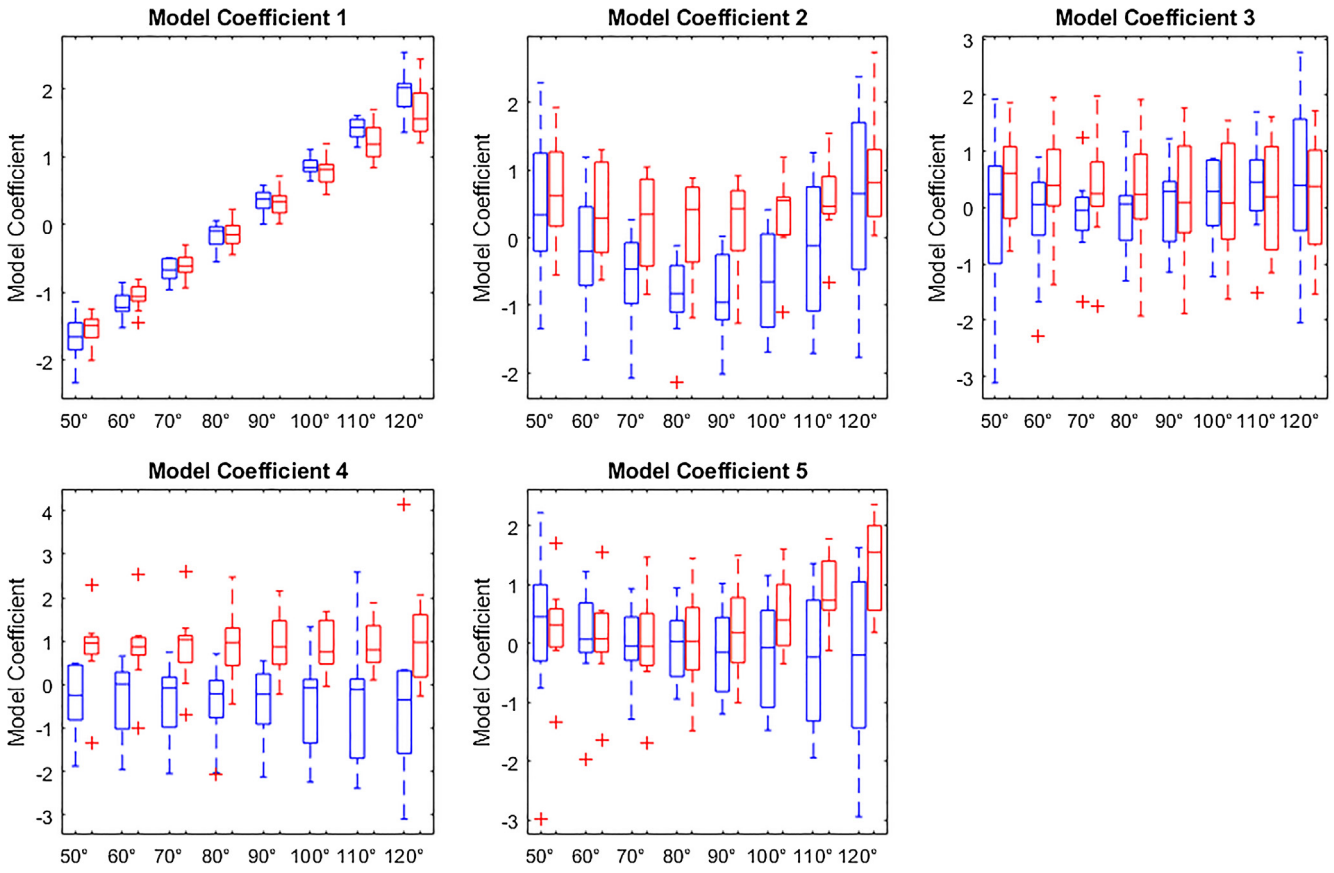

Fig. 9. Men are represented in blue while women are represented in red. A second order model was fitted for each volunteer to estimate how each wrist moved uniquely, and these models were sampled at eight RUD angles for comparison. Lower RUD angles refer to more radial deviation while higher RUD angles refer to more ulnar deviation. (For interpretation of the references to color in this figure legend, the reader is referred to the web version of this article.)

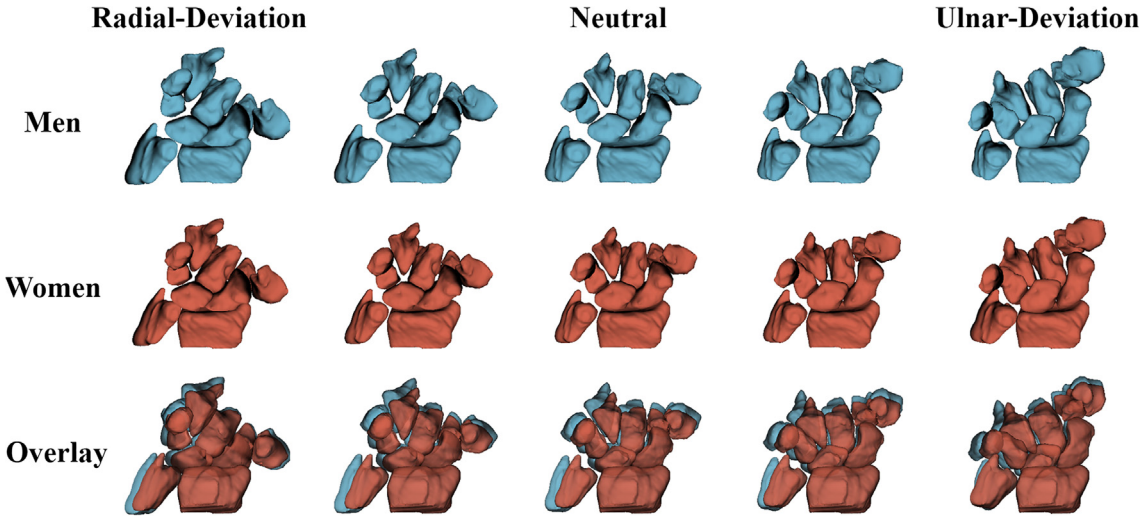

Fig. 10. The fitted models for men and women were sampled at five RUD angles and rendered above. The angles chosen were approximately the same as the five static positions a subset of the volunteers did during scanning. The main difference appears to be overall wrist scaling with men having larger wrists then women.

model coefficients, for each individual wrist. The ability of the basis functions to summarize wrist displacement comprehensively will help improve our understanding of the physiologically normal displacement of wrist tissues and for defining basis functions specifically for diagnosing, staging, quantifying, and longitudinally track wrist motion dysfunction. Several prospective applications of such knowledge could be considered, such as characterizing dynamic wrist instability (wrist bone malalignment during motion) (Garcia-Elias et al., 2014; Kuo and Wolfe, 2008; Lee et al., 2011), differences in symptomatic and asymptomatic participants with anatomical differences or variations, such as hyperlaxity or type 2 lunates (Abe et al., 2017; Borgese et al., 2017), and the outcomes of orthopaedic fusion, repair or reconstructive procedures (Walsh et al., 2002).

We demonstrated the utility of the approach for statistical comparison based on laterality (left versus right) and sex. We reject our first hypothesis that the model coefficients do not differ between the wrists of men and women, and we were able to identify both bone location-based and scaling differences via the proposed scheme. While previous studies have found overall scaling differences between bones of men and women (Chaudhari et al., 2014; Joshi et al., 2016; Neu et al., 2001; Schneider et al., 2015), after separating the groups, we found a descriptor sensitive to flexion-extension. This could be a by-product of the higher laxity presented by women compared to men (Garcia-Elias et al., 1995). Additionally, we confirmed our second hypothesis that the model coefficients did not differ for the right and left wrists of the same individual. Although we employed PCA-based eigen decomposition for extracting basis functions, it would also be possible in our framework to specify a different set of basis functions to study maneuvers. Our technique therefore could be easily extended to studies of other wrist maneuvers, a different subset of wrist bones, and to model bone displacement for other joints. Additionally, one of the basis functions could be specified to represent wrist scaling to reduce or remove any scaling component from the other basis functions.

The inter- and intra-subject variability in bone displacement makes creating robust models a difficult task. The proposed method is able to incorporate anatomical differences into the model by finding the most descriptive basis functions in a data-driven approach. The method was able to incorporate variations in overall wrist size (in the second basis function) and variations in bone displacement between the volunteers. There remains no consensus regarding normal carpal bone displacement during motion, and several theories have been proposed, such as the column (Taleisnik, 1976), row (Von Bonin, 1929), intercalated segment (Weber, 1984), and oval ring (Lichtman et al., 1981) concepts. Considering the complex and differential out-of-plane motions of the carpal bones, simplified models for wrist bone motion have been inaccurate (Crisco et al., 1999; Moojen et al., 2003; Werner et al., 1997; Wolfe et al., 2000). Cadaver studies have been conducted, however, only limited knowledge regarding wrist kinematics has be gleaned, as larger out-of-plane motions are found to occur *in vivo* than *in vitro* (Moojen et al., 2003). The statistical approach proposed has the benefit of being driven by data collected from the assessed cohort, and would enhance our understanding of bone displacement patterns on an ensemble level.

Considerable progress has been made in the acquisition of *in vivo* images during wrist motion. Published methods have used 2D static radiographs (Craigen and Stanley, 1995; Ferris et al., 2000), 3D static computed tomography (CT) (Crisco et al., 1999; Halilaj et al., 2014; Wolfe et al., 2000), and 3D static MRI (Fischer et al., 2011; Goto et al., 2005; Pillai et al., 2007). However, more recently, 4D (3D + time) imaging has become available via dynamic CT (Foumani et al., 2009; Garcia-Elias et al., 2014; Jais and Tay, 2017) and dynamic MRI (Boutin et al., 2013; Shaw et al., 2017). Our proposed method can employ these novel scanning approaches, to further refine the basis functions and to add to our current knowledge of wrist kinematics. A second-order polynomial model was chosen in order to allow for non-linear bone displacement interpolation for this initial bone trajectory estimation. It may become possible in the future to use such dynamic wrist imaging (such as CT or MRI) to further explore and refine this choice.

Our proposed technique may have potential applications in orthopaedic treatment selection and planning. Patients with pathological conditions such as carpal instabilities (i.e. scapholunate, lunotriquetral, and midcarpal instabilities) can be studied to see how their carpus kinematics differ from healthy normal bone trajectories before and after a reconstructive procedure (Shores et al., 2013). Lastly, the ability of this technique to focus on a specific subset of bones as a group (please see supplementary materials), or the displacement of a specific bone with respect to another bone, is a potentially important advantage as this may allow for tailoring reconstructive procedures. The modeling of a subset of bones could be interesting in assessing surgical procedures, such as fusion (Wolfe et al., 2000).

In our data-driven approach, while model coefficients (e.g., the 2nd) appeared to capture overall wrist scaling, we did not explicitly separate contributions of scaling of bone size versus bone displacement. In future work, we plan to compute independent models for each sex and further understand the contributions of bone scaling and displacement. To facilitate this, one of the basis functions could be specified to represent wrist scaling alone and potentially reduce scaling contributions from other basis functions. Although our focus in this study was to identify basis functions of the wrist to represent unassisted RUD maneuver, the method can be expanded to analyze the wrist under stress and during different maneuvers (e.g. RUD, flexion-extension, dart thrower, circumduction, etc.) using a similar methodology. These analyses would lead to a more comprehensive description of any wrist maneuver and abnormality.

The volunteers in our study were instructed to move their wrists to the neutral position and extreme positions in an unassisted manner. The wrist was unconstrained, except for the flat surface underneath it, with the aim of having more natural wrist positions. As a result, a variety of natural wrist angles for the static positions were obtained. We normalized for this by measuring the RUD angle of the wrist, and only after that, a clear and predictable path through eigenspace was more apparent. Another limitation was that we employed wrist segmentations from a single participant as a template, but utilizing probabilistic templates in future work may increase modeling accuracy.

5. Conclusions

We demonstrated the effectiveness of a PCA-based modeling scheme for statistical assessment of the trajectories of the bones of the wrist during the performance of a common wrist maneuver in each sex. We determined basis functions using bones displacement, showed their utility in comparing the right and left wrist bone displacement during maneuvers, presented application of modeling to an individual's wrist, and created a model of a subset of the wrist bones. Using our approach, the many degrees of freedom from the displacement of the ten bones of the wrist can be represented by just 5 basis functions that explain over 91% of variation across individuals. Additionally, these basis functions were able to predict intermediate bone position with high accuracy. Our proposed approach may aid in unifying theories of wrist kinematics and identify abnormal wrist pathologies with a higher sensitivity.

Conflict of interest

The authors have no conflict of interest to disclose.

Acknowledgment

The authors acknowledge the contributions by Marissa Borgese, Gerald Sonico, and Dr. Costin Tanase, all of our institution. This work was supported by grants from the National Science Foundation (NSF) (GRFP Grant No. 1650042), and the National Institutes of Health (NIH) (K12 HD051958 and R03 EB015099). The content is

solely the responsibility of the authors and does not necessarily represent the official views of the NSF or the NIH.

Appendix A. Supplementary material

Supplementary data associated with this article can be found, in the online version, at https://doi.org/10.1016/j.jbiomech.2019.01.030.

References

Abe, S., Moritomo, H., Oka, K., Sugamoto, K., Kasubuchi, K., Murase, T., Yoshikawa, H., 2017. Three-dimensional kinematics of the lunate, hamate, capitate and triquetrum with type 1 or 2 lunate morphology. J. Hand Surg. (Eur. Vol.). 1753193417744420.

Benjamini, Y., Hochberg, Y., 1995. Controlling the false discovery rate: a practical and powerful approach to multiple testing. J. Roy. Stat. Soc. Ser. B (Methodol.), 289–300.

Borgese, M., Boutin, R.D., Bayne, C.O., Szabo, R.M., Chaudhari, A.J., 2017. Association of lunate morphology, sex, and lunotriquetral interosseous ligament injury with radiologic measurement of the capitate-triquetrum joint. Skeletal Radiol. 46, 1729–1737.

Boutin, R.D., Buonocore, M.H., Immerman, I., Ashwell, Z., Sonico, G.J., Szabo, R.M., Chaudhari, A.J., 2013. Real-time magnetic resonance imaging (mri) during active wrist motion initial observations. PloS One 8, e84004.

Chaudhari, A.J., Leahy, R.M., Wise, B.L., Lane, N.E., Badawi, R.D., Joshi, A.A., 2014. Global point signature for shape analysis of carpal bones. Phys. Med. Biol. 59, 961.

Chen, X., Graham, J., Hutchinson, C., Muir, L., 2013. Automatic inference and measurement of 3d carpal bone kinematics from single view fluoroscopic sequences. IEEE Trans. Med. Imaging 32, 317–328.

Coburn, J.C., Upal, M.A., Crisco, J.J., 2007. Coordinate systems for the carpal bones of the wrist. J. Biomech. 40, 203–209.

Craigen, M., Stanley, J., 1995. Wrist kinematics: row, column or both? J. Hand Surg. 20, 165–170.

Crisco, J.J., McGovern, R.D., Wolfe, S.W., 1999. Noninvasive technique for measuring in vivo three-dimensional carpal bone kinematics. J. Orthopaed. Res. 17, 96–100.

Ferris, B.D., Stanton, J., Zamora, J., 2000. Kinematics of the wrist. Bone Joint J. 82, 242–245.

Fischer, K.J., Johnson, J.E., Waller, A.J., McIff, T.E., Toby, E.B., Bilgen, M., 2011. Mri-based modeling for radiocarpal joint mechanics: validation criteria and results for four specimen-specific models. J. Biomech. Eng. 133, 101004.

Fisher, A., Caffo, B., Schwartz, B., Zipunnikov, V., 2016. Fast, exact bootstrap principal component analysis for p> 1 million. J. Am. Stat. Assoc. 111, 846–860.

Foster, B., Joshi, A.A., Borgese, M., Abdelhafez, Y., Boutin, R.D., Chaudhari, A.J., 2017. WRIST-A WRist Image Segmentation Toolkit for Carpal Bone Delineation from MRI. Comput. Med. Imaging Graph.

Foumani, M., Strackee, S., Jonges, R., Blankevoort, L., Zwinderman, A., Carelsen, B., Streekstra, G., 2009. In-vivo three-dimensional carpal bone kinematics during flexion–extension and radio–ulnar deviation of the wrist: dynamic motion versus step-wise static wrist positions. J. Biomech. 42, 2664–2671.

Galley, I., Bain, G.I., McLean, J.M., 2007. Influence of lunate type on scaphoid kinematics. J. Hand Surg. 32, 842–847.

Garcia-Elias, M., Alomar Serrallach, X., Monill Serra, J., 2014. Dart-throwing motion in patients with scapholunate instability: a dynamic four-dimensional computed tomography study. J. Hand Surg. (Eur. Vol.) 39, 346–352.

Garcia-Elias, M., Ribe, M., Rodriguez, J., Cots, M., Casas, J., 1995. Influence of joint laxity on scaphoid kinematics. J. Hand Surg. 20, 379–382.

Goto, A., Moritomo, H., Murase, T., Oka, K., Sugamoto, K., Arimura, T., Masumoto, J., Tamura, S., Yoshikawa, H., Ochi, T., 2005. In vivo three-dimensional wrist motion analysis using magnetic resonance imaging and volume-based registration. J. Orthop. Res. 23, 750–756.

Halilaj, E., Rainbow, M.J., Got, C., Schwartz, J.B., Moore, D.C., Weiss, A.-P.C., Ladd, A.L., Crisco, J.J., 2014. In vivo kinematics of the thumb carpometacarpal joint during three isometric functional tasks. Clin. Orthopaed. Relat. Res.® 472, 1114–1122.

Heimann, T., Meinzer, H.-P., 2009. Statistical shape models for 3d medical image segmentation: a review. Med. Image Anal. 13, 543–563.

Jais, I.M., Tay, S., 2017. Kinematic analysis of the scaphoid using gated four-dimensional ct. Clin. Radiol.

Joshi, A.A., Leahy, R.M., Badawi, R.D., Chaudhari, A.J., 2016. Registration-based morphometry for shape analysis of the bones of the human wrist. IEEE Trans. Med. Imaging 35, 416–426.

Kawanishi, Y., Oka, K., Tanaka, H., Sugamoto, K., Murase, T., 2017. In vivo scaphoid motion during thumb and forearm motion in casts for scaphoid fractures. J. Hand Surg. 42, 475–e1.

Kuo, C.E., Wolfe, S.W., 2008. Scapholunate instability: current concepts in diagnosis and management. J. Hand Surg. 33, 998–1013.

Lee, S.K., Desai, H., Silver, B., Dhaliwal, G., Paksima, N., 2011. Comparison of radiographic stress views for scapholunate dynamic instability in a cadaver model. J. Hand Surg. 36, 1149–1157.

Lichtman, D.M., Schneider, J.R., Swafford, A.R., Mack, G.R., 1981. Ulnar midcarpal instability-clinical and laboratory analysis. J. Hand Surg. 6, 515–523.

Moojen, T.M., Snel, J.G., Ritt, M.J., Venema, H.W., Kauer, J.M., Bos, K.E., 2003. In vivo analysis of carpal kinematics and comparative review of the literature. J. Hand Surg. 28, 81–87.

Neu, C., Crisco, J., Wolfe, S., 2001. In vivo kinematic behavior of the radio-capitate joint during wrist flexion–extension and radio-ulnar deviation. J. Biomech. 34, 1429–1438.

Pillai, R.R., Thoomukuntla, B., Ateshian, G.A., Fischer, K.J., 2007. Mri-based modeling for evaluation of in vivo contact mechanics in the human wrist during active light grasp. J. Biomech. 40, 2781–2787.

Rainbow, M., Wolff, A., Crisco, J., Wolfe, S., 2016. Functional kinematics of the wrist. J. Hand Surg. (Eur. Vol.) 41, 7–21.

Rainbow, M.J., Crisco, J.J., Moore, D.C., Wolfe, S.W., 2008. Gender differences in capitate kinematics are eliminated after accounting for variation in carpal size. J. Biomech. Eng. 130, 041003.

Rainbow, M.J., Kamal, R.N., Leventhal, E., Akelman, E., Moore, D.C., Wolfe, S.W., Crisco, J.J., 2013. In vivo kinematics of the scaphoid, lunate, capitate, and third metacarpal in extreme wrist flexion and extension. J. Hand Surg. 38, 278–288.

Sandow, M., Fisher, T., Howard, C., Papas, S., 2014. Unifying model of carpal mechanics based on computationally derived isometric constraints and rules-based motion–the stable central column theory. J. Hand Surg. (Eur. Vol.) 39, 353–363.

Schneider, M., Zhang, J., Crisco, J., Weiss, A., Ladd, A., Nielsen, P., Besier, T., 2015. Men and women have similarly shaped carpometacarpal joint bones. J. Biomech. 48, 3420–3426.

Shaw, C., Foster, B., Boutin, R., Szabo, R., Bayne, C., Nayak, K., Chaudhari, A., 2017. Comparison of real-time mri pulse sequences for tracking tissues of the actively moving wrist. Am. Soc. Biomech. (ASB).

Shores, J.T., Demehri, S., Chhabra, A., 2013. Kinematic 4 dimensional ct imaging in the assessment of wrist biomechanics before and after surgical repair. Eplasty, 13.

Sonenblum, S.E., Crisco, J.J., Kang, L., Akelman, E., 2004. In vivo motion of the scaphotrapezio–trapezoidal (stt) joint. J. Biomech. 37, 645–652.

Stegmann, M.B., Gomez, D.D., 2002. A brief introduction to statistical shape analysis. Inform. Math. Model., Technical Univ. Denmark, DTU 15.

Taleisnik, J., 1976. The ligaments of the wrist. J. Hand Surg. 1, 110–118.

Von Bonin, G., 1929. A note on the kinematics of the wrist-joint. J. Anat. 63, 259.

Walsh, J.J., Berger, R.A., Cooney, W.P., 2002. Current status of scapholunate interosseous ligament injuries. JAAOS-J. Am. Acad. Orthopaed. Surg. 10, 32–42.

Waters, M.S., Werner, F.W., Haddad, S.F., McGrattan, M.L., Short, W.H., 2016. Biomechanical evaluation of scaphoid and lunate kinematics following selective sectioning of portions of the scapholunate interosseous ligament. J. Hand Surg. 41, 208–213.

Weber, E., 1984. Concepts governing the rotational shift of the intercalated segment of the carpus. Orthoped. Clin. North Am. 15, 193–207.

Werner, F.W., Short, W.H., Fortino, M.D., Palmer, A.K., 1997. The relative contribution of selected carpal bones to global wrist motion during simulated planar and out-of-plane wrist motion. J. Hand Surg. 22, 708–713.

Werner, F.W., Sutton, L.G., Allison, M.A., Gilula, L.A., Short, W.H., Wollstein, R., 2011. Scaphoid and lunate translation in the intact wrist and following ligament resection: a cadaver study. J. Hand Surg. 36, 291–298.

Wold, S., Esbensen, K., Geladi, P., 1987. Principal component analysis. Chemometr. Intell. Lab. Syst. 2, 37–52.

Wolfe, S.W., Neu, C., Crisco, J.J., 2000. In vivo scaphoid, lunate, and capitate kinematics in flexion and in extension. J. Hand Surg. 25, 860–869.

Wu, G., Van der Helm, F.C., Veeger, H.D., Makhsous, M., Van Roy, P., Anglin, C., Wang, X., 2005. Isb recommendation on definitions of joint coordinate systems of various joints for the reporting of human joint motion-part ii: shoulder, elbow, wrist and hand. J. Biomech. 38, 981–992.

Xia, Y., Fripp, J., Chandra, S.S., Schwarz, R., Engstrom, C., Crozier, S., 2013. Automated bone segmentation from large field of view 3d mr images of the hip joint. Phys. Med. Biol. 58, 7375.